Vacuum 85 (2010) 48–54

Contents lists available at ScienceDirect

Vacuum

journal homepage: www.elsevier.com/locate/vacuum

# Numerical analysis in focusing characteristics of the three-dimensional trapezoidal electrodes for carbon nanotube field emitters

Faheng Zang, Guifu Ding*, Yan Wang, Min Deng

*Key Laboratory for Thin Film and Microfabrication Technology of Ministry of Education, National Key Laboratory of Micro/Nano Fabrication Technology, Research Institute of Micro/Nano Science and Technology, Shanghai Jiao Tong University, 800 Dongchuan Road, Shanghai 200240, People's Republic of China*

ARTICLE INFO

*Article history:*
Received 21 October 2009
Received in revised form
8 March 2010
Accepted 13 March 2010

*Keywords:*
Field emission
Focusing electrode
Fowler–Nordheim equation
FDTD
PIC

ABSTRACT

In this study, the focusing characteristics of three-dimensional trapezoidal focusing electrodes for carbon nanotube field emitters are analyzed by the combination of the finite-difference time-domain and particle-in-cell methods. To investigate the divergences of the electrons, the three-dimensional trajectories of the electron beams are simulated by evaluating the electrons' positions and momentums. The divergence angles of electrons in the emitters with three-dimensional focusing electrodes are proved to be smaller than those with the conventional triode structure or with the planar focusing electrodes. Characteristics of the 4 μm-thick three-dimensional geometries (trapezoidal, rectangular and inversed trapezoidal) are compared. The 1 V biased three-dimensional trapezoidal focusing electrode is optimal in regulating the divergence of the beams and forming uniform electron spots on the anode. The average divergence angle of the electrons is limited to 0.1309 rad on the anode plane while the maximum divergence angle is 0.3236 rad.



## 1. Introduction

The field emitters are among the booming vacuum microelectronic devices in recent decades. Compared with the conventional thermal electron emitters, field emitters are excellent in smart size, non heat-up process, low power consumption and insensitivity to the temperature fluctuation. Since the discovery of carbon nanotube (CNT) [1], the CNT is proved to be a promising material for fabrication of field emission cathodes because of its small tip ratio and low work function. Attribute to the CNT's excellent field emission (FE) property [2], the CNT-based field emission cathodes are developed for cold-field emission devices [3–5].

The current density and beam convergence are two critical factors for a good field emitter. To obtain high current density on the anode, the arrayed CNT emission sources and the triode structure (anode, gate and cathode electrodes) are developed [6,7]. In these design, the electrons are accelerated in the typical triode emitters by applying high voltage on anode plane. Thus, the trajectory time is compressed by the acceleration of the electrons caused by the axial field. However, this design was unable to regulate the beam divergence because the generated field has little transverse component. In the field emission displays (FED), which requires high isolation between pixels, the overlapping between units caused by electron beam divergence should be avoid. The focusing electrodes above the gate and associating electrodes paralleled to the cathodes are designed as attempts to improve the convergence of emitted electron beams [8–10]. Currently, the focusing electrodes are mainly planar structured with the thickness of 150–300 nm.

The trajectory of the electron beams is the main indication for beam divergence; however, it can hardly be observed in experiments. Numerical methods are then introduced in analyzing the FE properties of the CNT-based field emitters and the trajectory of the beams. The local field enhancement is studied on the single nanotube tip by the two-dimensional examination of electric potential contours [11]. Further, the finite-difference time-domain method (FDTD) was combined with the particle-in-cell method (PIC) in the two-dimensional study of the relation between the CNT density and the current density for a certain emitter [12].

In this study, three major types of the three-dimensional focusing electrodes are designed, analyzed and compared. FDTD method is applied in calculation of the electromagnetic field in the emitters while the PIC method is used in evaluation of the trajectories in the three-dimensional simulation. Owing to the influence of the biased focusing electrodes, the convergence of the field induced electron beams transiting through the focusing electrodes was observed. Meanwhile, focusing characteristics of emitters with the three-dimensional focusing electrodes are studied and

* Corresponding author. Tel.: +86 21 34206689; fax: +86 21 34206686.
*E-mail address:* gfding@sjtu.edu.cn (G. Ding).

0042-207X/$ – see front matter © 2010 Elsevier Ltd. All rights reserved.
doi:10.1016/j.vacuum.2010.03.010

compared with those of the planar ones. The variable bias voltage (from 0 V to 8 V) on the focusing electrode was also investigated to approach the uniformity of the electron beams.

## 2. Design and methodologies

The prototype of the emitter with inversed trapezoidal three-dimensional focusing electrodes was successfully fabricated in the UV-LIGA process (Fig. 1(a)). The 4 μm-thick three-dimensional focusing electrodes were fabricated using electroplated nickel. The scanning electron microscope image showed that CNTs were dispersed uniformly and combined with Cu-matrix which formed the composite CNT emission arrays [13] (Fig. 1(b)). The average length of the exposed parts of the CNTs approximates to 500 nm by observation. The diameters of the implemented multi-walled CNTs were 20 μm with the tip ratio less than 5 μm.

The newly designed three-dimensional focusing electrodes were based on the fabricated prototype. In this study, the analysis aimed at the optimization of the focusing characteristics. For the parallel geometry of the emitter, as was shown in Fig. 1(a), the model was simplified to a $14 \times 10$ μm emission unit with the focusing electrodes on its two edges (Fig. 2(a)). Seven hexagonal pores on the gate formed a beehive structure which ensures high transit areas and the solidity of the structure (Fig. 2(a)). Effective transit areas of the gate were calculated to be 68.65% of the total gate area. Each CNT emission array was developed below the hexagonal gate pore. According to the fabrication process, we assumed the single CNT in the array was 500 nm in height and 800 nm paralleling to each other.

The three-dimensional focusing electrodes with different cross-sectional shapes- the trapezoidal (Type A), rectangular (Type B) and inversed trapezoidal (Type C) – were investigated (the contours were schemed in Fig. 2(b)). The hypotenuse obliquities of the trapezoidal and inversed trapezoidal electrodes are ±0.24 rad respectively. In addition, the emitter with conventional triode structure and that with the planar focusing electrodes (the thickness of the electrode was below 1 μm) were also compared with the designed three-dimensional focusing electrodes in the simulation.

The 4 μm-thick three-dimensional focusing electrodes were biased by variable focusing voltage ($V_F$) while the gate voltage ($V_G$) and anode voltage ($V_A$) were fixed to 9 V and 20 V respectively. The local electric field on the CNTs tips is 3 V/μm induced by $V_G$, which is critical for the field emission. Also, the accelerating field beyond the gate is 1 V/μm generated by $V_A$. The focusing voltage was configured as variable to adjust the focusing characteristics of the electrodes. The 0.5 μm-thick silicon nitride was sandwiched between the gate and focusing electrode as the dielectric for its high breakdown strength.

The focusing characteristics of electrodes were investigated by the illustration of the electron spots on anode plane. The transverse divergence angles and positions of the electrons are two critical factors in the investigation. Setting the origin of the working plane in the center of the anode, $\theta_m$ is defined as maximum divergence angle of the electron on the anode; $\theta_e$ is the divergence angle of the electron on the beam envelope. The transverse positions of the electrons with the maximum divergence and those on the beam envelope were defined as $r_m$ and $r_e$ respectively. To achieve the uniform emission beams, the average divergence angle ($\theta_{average}$) should also be minimized. Optimally, the beam spots on anode should cover the range of anode, which means $r_e$ were approximate to the half width of the unit (7 μm). Meanwhile, the electrons collisions on the focusing electrodes should be avoided to ensure a larger anode collect current density. Limited by the calculation resources, we set the number of electrons generated from each CNT tip as 47; and the total number of electrons investigated in this study was amounted to 2961.

The simulation process combined the FDTD and particle–mesh PIC methods (shown in Fig. 3). The FDTD method is one of the premier methods in analysis of electromagnetic field. As a grid-based method for electrodynamics problems, the FDTD method was implemented to solve the Maxwell equations in the emitter with initial boundary conditions. In isotropic medium, Maxwell's equations in differential form are as follows:

$$\nabla \times H = J + \frac{\partial D}{\partial t} \tag{1}$$

$$\nabla \times E = -\frac{\partial B}{\partial t} \tag{2}$$

$$\nabla \cdot D = \rho \tag{3}$$

$$\nabla \cdot B = 0 \tag{4}$$

The calculated fields on the grids were evaluated by space charges induced by emission currents in the iteration process. Since FDTD is a time-domain method, electromagnetic field is calculated on every grid and updated in the next time segment. This feature establishes the basis for the simulations of electrodynamics and electron tracing in the PIC method. The top and bottom boundaries of the unit were set as electrical for the existence of metal anode and cathode planes; and other boundaries were set as open spaces. In the initial calculation cycle, the field was established by the potentials on the biased anode, gate and focusing electrode without the influence of emitted electron beams. The electromagnetic fields on the meshed grids were calculated and stored. In order to illustrate the electrons trajectory, the electric fields between each calculated grids were numerically interpolated, and both momentum and position of the electron were evaluated according to the interpolated fields. The

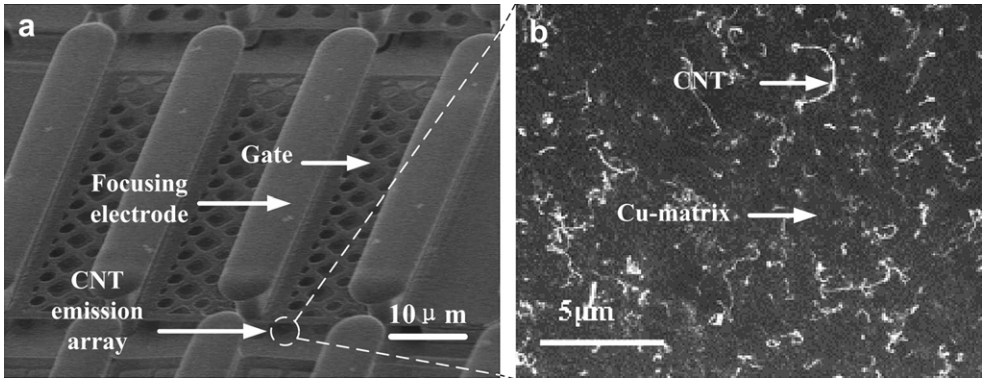


**Fig. 1.** SEM images of (a) the field emitter with three-dimensional focusing electrode and (b) the composite CNTs with Cu-matrix on the emission array [13].

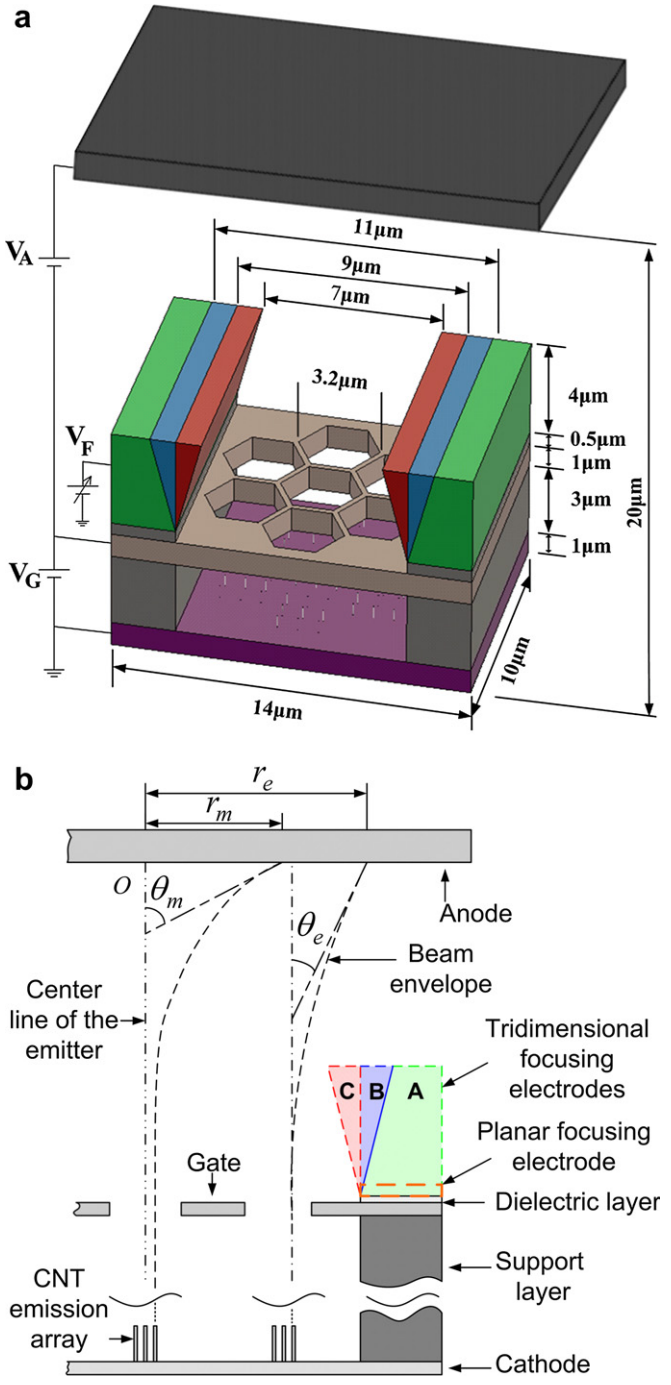


**Fig. 2.** (a) Three-dimensional geometry and (b) cross-sectional scheme of the simulation unit.

governing equations of the momentum and position evaluation of the field induced electrons are:

$$\frac{\mathrm{d}(m\vec{v})}{\mathrm{d}t} = e(\vec{E} + \vec{v} \times \vec{B}) \tag{5}$$

$$\frac{\mathrm{d}\vec{r}}{\mathrm{d}t} = \vec{v} \tag{6}$$

In the computational analysis, the analytic equations were placed with discrete forms:

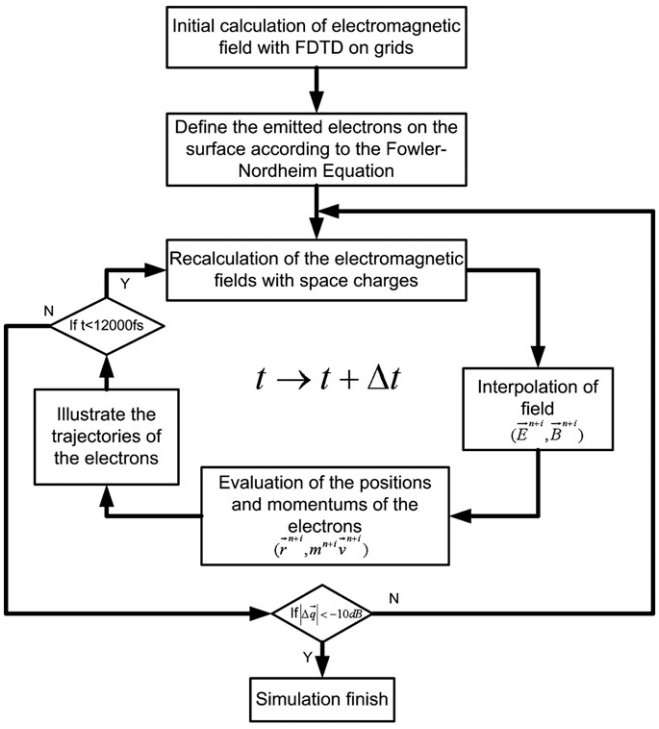


**Fig. 3.** The simulation process with FDTD-PIC methods.

$$m^{n+2i}\vec{v}^{n+2i} = m^n v^n + e\Delta t\left(\vec{E}^{n+i} + \vec{v}^{n+i} \times \vec{B}^{n+i}\right) \tag{7}$$

$$\vec{r}^{n+3i} = \vec{r}^{n+i} + \Delta t\,\vec{v}^{n+2i} \tag{8}$$

$$|\Delta\vec{q}| = \frac{|\vec{q}^n - \vec{q}^{n+1}|}{|\vec{q}^n|} \tag{9}$$

Where $\vec{E}^{n+i}$ and $\vec{B}^{n+i}$ are interpolated electric and magnetic field from the calculated fields on the grids. By consistently evaluating the electron's velocity and position in $\Delta t$, we illustrate the trajectories of the emitted electrons in the total simulation period (12,000 fs). As we assume the stable state is established, the trajectories were then used to determine the space charges of the emission electrons and set as conditions for evaluation of electric field in iteration. The iteration stops if the deviation of space charge $|\Delta\vec{q}|$ is below −10 dB.

In the analysis, only the electron–mesh interactions were concerned; meanwhile, the electromagnetic fields are only redefined on the established mesh with the additional condition of spaces charges. The PIC method which involves re-meshing and particle–particle interactions is relatively more accurate especially in electrodynamics analysis of fluidics problems such as plasma simulation; however, it suffers from large expenses in resources and time especially in three-dimensional simulations if grids are kept updated. In our study, since the emitter is vacuumed, the movement of electrons can be simplified as parabolic governed by established fields and space charges. Therefore, the PIC process with electron–mesh interactions on fixed grids can achieve high accuracy, short computing cycle and low resource expenses in the three-dimensional analysis of the focusing characteristics.

The current density on the nanotube surface was determined by Fowler–Nordheim equation [2]:

$$J = a\frac{F^2}{\varphi}\exp\left(-\frac{b\varphi^{\frac{3}{2}}}{F}\right) \quad (10)$$

In the equation (10), $F = \beta E$ is the local electric field on CNT tip and $E = U/d$ is the background field induced by biased electrodes. The value of enhancement parameter ($\beta$) varies from different emission materials and tip ratios; $a$ and $b$ are constants which are defined as,

$$a \equiv e^3/8\pi h_p = 1.54 \times 10^{-6}\left[AeVV^{-2}\right] \quad (11)$$

$$b \equiv \frac{8\pi}{3}(2m_e)^{\frac{1}{2}}/eh_p = 6.83 \times 10^9\left[VeV^{-\frac{3}{2}}m^{-1}\right] \quad (12)$$

The work function for multi-walled CNTs is typically 4.6–4.8 eV [3]. In this study, we defined $\varphi$ of the multi-walled CNTs as 4.8 eV. The Fowler–Nordheim equation established the relationship between the electric field and emission current density on the emission tips. It was used to determine the current density on the nanotubes' surfaces in the electron trajectory simulation.

## 3. Results and discussion

The development of the focusing electrode is to regulate the divergent effects of the field emission electron beams in order to achieve uniform beam spots on anode electrode plane without overlapping between units. In the conventional triode structures, overlapping is inevitable due to the dispersion of electron beams caused by transverse electrostatic forces induced by the gate (Fig. 4 (a)). Planar focusing electrodes could not effectively regulate the divergence because their induced electric field can only reach the beams on the edge of the units. In comparison, the field induced by the biased three-dimensional focusing electrode can effectively minimize the divergence angles of the electrons, which helps to form the uniform beams. Point clouds, which show the relations between electron positions ($r$) and divergence angles ($\theta$) of three different types of focusing electrode, are depicted in Fig. 4(b). The focusing voltage was set as 1 V identically for each type of the emitters.

For the emission unit without focusing electrode, electron beams diverged severely; and the beams cover the range from −12.2 to 12.3 μm on the anode. Since the geometric range of the emission unit was −7–7 μm, the overlapping range between the units was 5.3 μm. For the unit with planar focusing electrodes, the electron spots on anode ranged from −9 μm to 9.5 μm; and the overlapping range decreased to about 2.5 μm. In Fig. 4(a), the three-dimensional rectangular focusing electrode effectively regulated the divergence of the beam; and the overlapping was avoided. The focusing characteristics of three prime types of three-dimensional focusing electrodes (trapezoidal, rectangular and inversed trapezoidal) were compared by spotting the electrons on anode (Fig. 4(b)). Analyzed by fourth-order polynomial fittings of the point clouds, the uniformity of the beams in the unit with trapezoidal focusing electrode was superior those in the other two counterparts. It was because the divergence angles increased more smoothly versus transverse positions. For trapezoidal focusing electrodes, the electron spots ranged from −7.3 μm to 7.46 μm in transverse direction which covered the geometric ranges of the unit without severe overlapping. The parameters which symbol the focusing characteristics of the discussed geometries were listed in Table 1.

It was reconfirmed in Table 1 that the focusing characteristics of trapezoidal focusing electrode were superior: it held the smallest

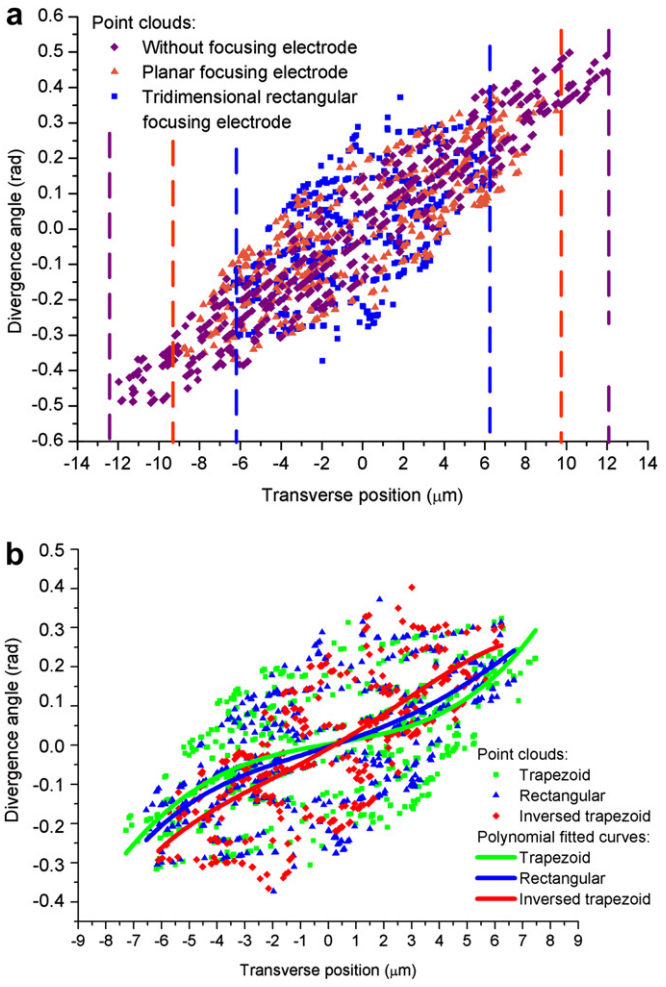


**Fig. 4.** Point clouds of beam spots on anode in the emission units (a) without, with planar and three-dimensional rectangular focusing electrodes; (b) with trapezoidal, rectangular and inversed trapezoidal focusing electrodes.

values of $\theta_m$ (0.3236 rad) and $\theta_e$ (0.1306 rad) respectively which denoted the electron beams regulated by trapezoidal electrode were uniform.

The electron collision on focusing electrodes should be avoided because it diminishes the number of electrons reached the anode and thus attenuate the collection current density. Given the identical numbers of induced electrons in the simulations, the minimal electron collisions of 46 on focusing electrode and maximal collisions of 566 on anode were achieved simultaneously in trapezoidal focusing electrode. The overlapping region was slight (0.46 μm between units), which ensures the isolation between the units.

With either rectangular or inversed trapezoidal electrodes, the central beams were over influenced by focusing electrode induced electric field, which resulted in the appearances of maximum diverged electrons in the central of the units. Also, since $r_e$ was smaller than 7 μm, there would be electron vacancy between units.

Based on the analysis, the trapezoidal was selected as optimal geometry for three-dimensional focusing electrode design and was further examined by increasing voltage bias. The bias increased from 0 V to 8 V with the step of 0.25 V. The relations of parameters ($\theta_m$, $\theta_e$, $r_m$ and $r_e$) with the bias voltages were plotted in Fig. 5.

**Table 1**
Focusing characteristics of different focusing electrodes.

| Focusing electrode types | $\theta_m$ (rad) | $r_m$ (μm) | $\theta_e$ (rad) | $r_e$ (μm) | $\theta_{average}$ (rad) | Electrons collide on focusing electrodes | Electrons collide on anode |
|---|---|---|---|---|---|---|---|
| Without | 0.4988 | 10.1589 | 0.4452 | 11.9931 | 0.2308 | – | 637 |
| Planar | 0.3741 | 6.3770 | 0.3338 | 9.5048 | 0.1547 | 10 | 587 |
| Trapezoidal | 0.3236 | 6.2437 | 0.2218 | 7.4601 | 0.1309 | 46 | 566 |
| Rectangular | 0.3728 | 1.9742 | 0.1667 | 6.6807 | 0.1397 | 70 | 505 |
| Inversed trapezoidal | 0.4029 | 3.0013 | 0.3036 | 6.2283 | 0.1467 | 270 | 401 |

The maximum divergence angle ($\theta_m$) decreased as the bias voltage was increased from 0 V to 1 V, and it arrived at its nadir when biased by 1 V DC. From 1 V to 5.75 V, the $\theta_m$ increased smoothly. And it increased steeply when the bias voltage is 5.75–8 V (Fig. 5(a)). Divergence angle of the electrons on the beam envelope ($\theta_e$) increased in the voltage ranges of 0–2.75 V and 3–8 V. $\theta_e$ diminished sharply as the bias voltages increased from 2.75 V to 3 V. The reason for this sharp decrease is the change in electric fields: when the bias voltage on focusing electrode is below 2.75 V, the electric field between the gates and focusing electrodes are stronger than the field between gates and cathode. The electrons, especially those in the center of the beams, were greatly affected by the strong transverse field beyond the gates. However, as bias voltage on focusing electrodes continue to increase, electric field between the gates and focusing electrodes are less influential to the electrons in the center of the beams; so, divergence of the central electrons diminished which lead to the sharp decrease of $\theta_e$ as was shown in Fig. 5(a).

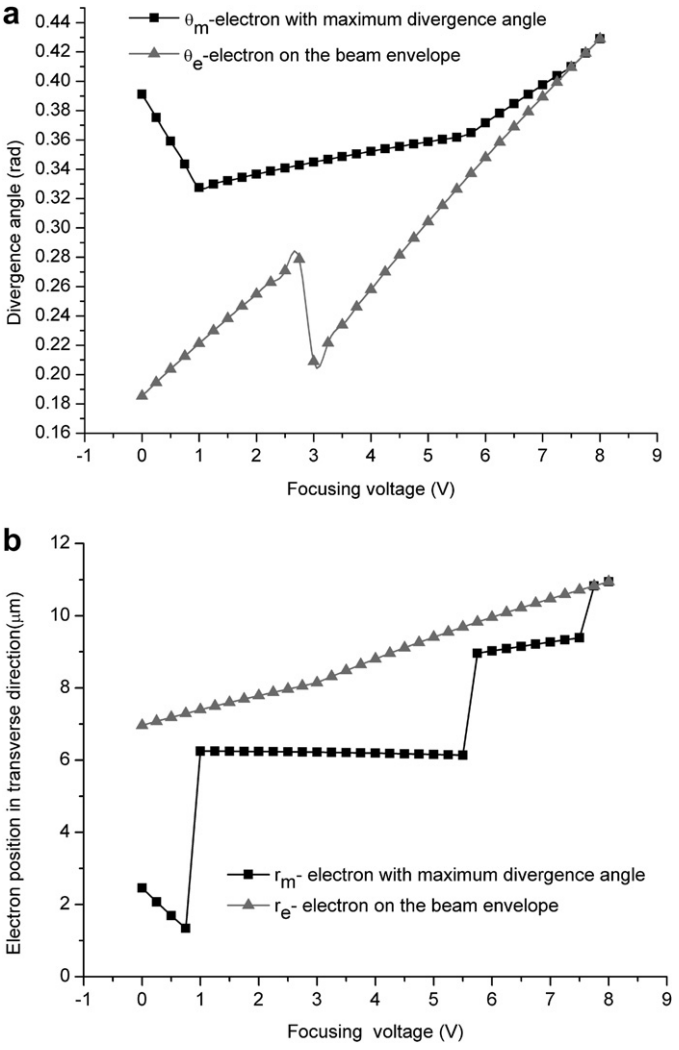


**Fig. 5.** (a) Divergence angles and (b) transverse position of the electrons on anode in the emission unit with trapezoidal focusing electrode biased by increasing focusing voltages.

The ladder-like plots of $r_m$ in Fig. 5(b) was result from the discrete dispersion of CNT arrays in the model. The CNTs were not dispersed continuously in the unit. There were seven discrete CNT arrays in the model (one was in the center; two were in the terminal of the central line; four were in the margins). There were gaps between each array. Besides, the gate also obstructed some of the electrons emitted from the arrays, which caused the discontinuity of electron beams.

The geometric discontinuity also caused the differences in field on each CNT emission array. When focusing voltage was low, the electrons from the central array collided on the anode with the maximum divergence angle. As the voltage increase, the field was weakened; and electrons emitted from the marginal CNT arrays, which collided on the outer anode, became the most diverged ones. Therefore, every discontinuity point on the plot symbols that the maximum diverged electrons emitted altered from one CNT array to another.

The position of electrons on the beam envelope $r_e$ was determined by the electrons emitted from the marginal CNT array. It increased continuously from 7 μm to about 11 μm with the increase of bias voltage (Fig. 5(b)). With the focusing voltage ranging from 7.75 V to 8 V, the values of $r_e$ and $r_m$ are identical because the maximum diverged electrons are on the envelope.

In the analysis, the silicon nitride dielectric layer was sandwiched between the focusing unit and gate. And, it is located in the margins of the unit. So, it can be simplified as a parallel-plate capacitor. This ensured that the electric field in the layer will not greatly affect the electron beams in the unit. The biased trapezoidal focusing electrode generated a strong electric field pointing on the hypotenuse surface of the electrode. The electric force on electrons pointed to the center of the unit and regulated the transverse divergence of the electron beams (shown in Fig. 6(a)).

Trajectories of the electrons emitted from CNT arrays were simulated by FDTD and PIC methods (demonstrated in Fig. 6(b)). When the electrons arrived on the anode, the kinetic energy increased to the approximate 27 eV. Beams in the center of the unit are symmetrically affected by focusing electrodes on the both edges, and the divergences are relatively slight. Electrons on the marginal parts of these beams show clear deflexions with their momentums decreased from 12 eV to the approximated 7 eV (Fig. 6(c)). Beams in the marginal parts of the unit, however, were asymmetrically affected by the two focusing electrodes, and the beams were deviated to the other side of unit with relatively large divergence angles (Fig. 6(d)). Thus, it can be concluded that the beams in the marginal parts of the unit were the main sources of the diverged beams in the emitter with 1 V biased trapezoidal focusing electrode.

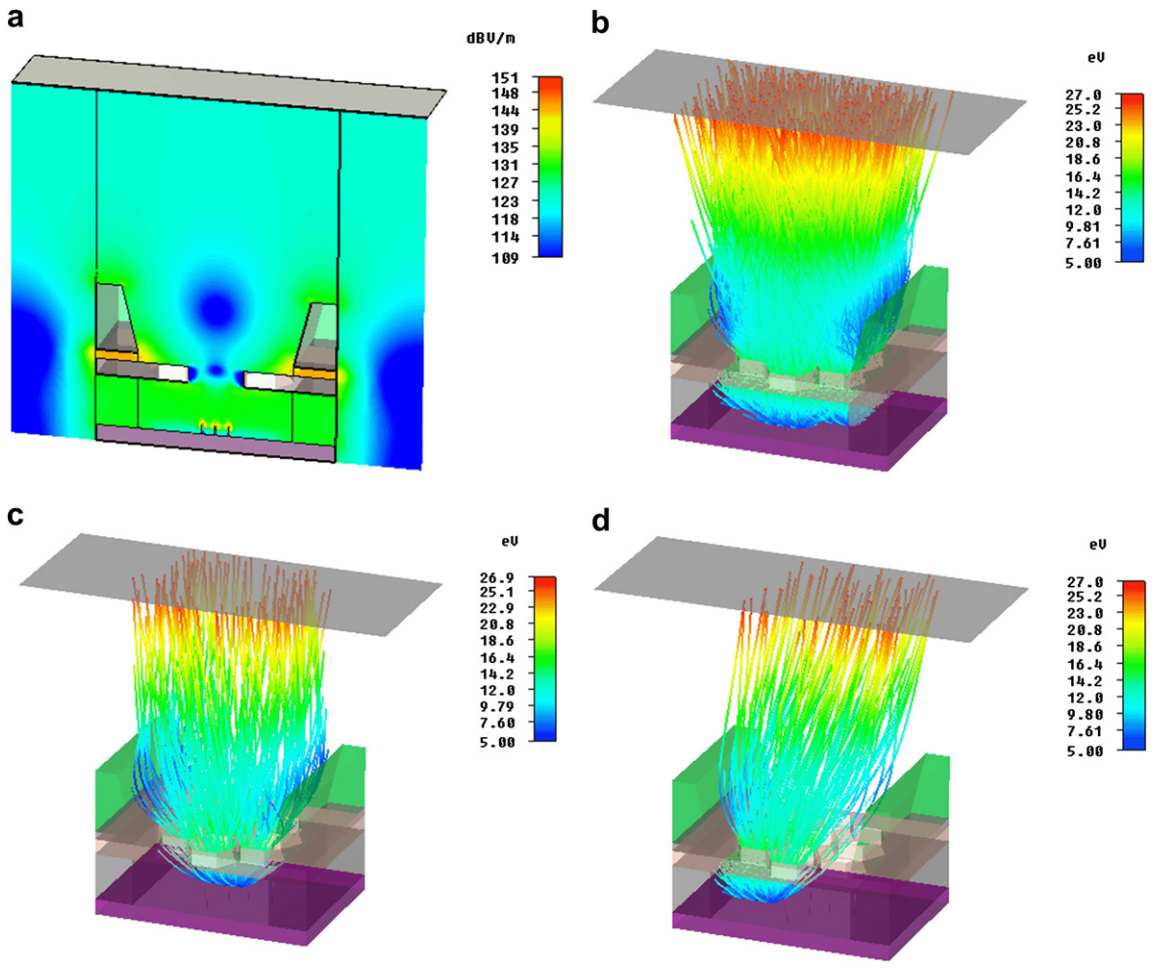


**Fig. 6.** (a) Contour of electric field magnitude on the cross-section of the emission unit with trapezoidal focusing electrode; (b) trajectory of beams in the emission unit; (c) trajectory of the beams emitted from the central CNT array and (d) those from the marginal CNT array.

## 4. Conclusion

The focusing characteristics of three-dimensional focusing electrodes in the CNT field emitters are analyzed using FDTD and PIC methods. The FDTD-PIC iteration is used to calculate the electromagnetic field on the meshed grids with space charge induced by the emission electrons. Trajectories of the emitted electrons are calculated by evaluating the positions and momentums using PIC method. Compared with the emitter without focusing electrodes or with planar focusing electrodes, the three-dimensional focusing electrodes are proved to be superb in regulating the divergence of the electron beams. The influence of focusing electrode is strong when the bias voltage is low. In the center of the unit, electrons are over influenced and diverge greatly when the focusing voltage is below 1 V. For the electron on the beam envelope, there is a sharp decline of divergence angle when the focusing voltage is 2.75–3 V.

In general, the 1 V biased three-dimensional trapezoidal focusing electrode is optimal to form the uniform electron beams. The maximum and average divergence angles of the electrons in this condition are 0.3236 rad and 0.1309 rad respectively. Overlapping between the units is controlled to 0.46 μm. As the electron spots cover the range of anode, the vacancy of electron beams between the units is eliminated. Electron beams emitted from the center of the unit are more uniform; and the trajectories are distributed symmetrically.

## Acknowledgement

The work was supported by the High-tech Research and Development Program of China (Grant No. 2006AA04Z308), the Shanghai Special Nano Foundation (Grant No. 0952nm06300) and the Chinese National Natural Science Foundation (50775148, 50675139).

## References

[1] Iijima Sumio. Helical microtubules of graphitic carbon. Nature 1991;354:56–8.
[2] Fowler RH, Nordheim L. Electron emission in intense electric fields. Proc R Soc London A 1928;119(781):173–81.
[3] Gao Ruiping, Pan Zhengwei, Wang Zhong L. Work function at the tips of multiwalled carbon nanotubes. Appl Phys Lett 2001;78(12):1757–9.
[4] Waltde Heer A, Châtelain A, Ugarte D. A carbon nanotube field-emission electron source. Science 1995;270(5239):1179–80.
[5] Lan Yung-Chiang, Hu Yuan, Lin Tsang-Lang, Chuang Feng-Yu, Tsai Jyun-Hwei, Lee Cheng-Chung, et al. Simulation study of reflective-type carbon nanotube field emission display. Jpn J Appl Phys 2002;41:657–63.
[6] Ho Park Kyung, Jong Seo Woo, Lee Soonil, Koh Ken Ha. Triode field emitter with a gated planar carbon-nanoparticle cathode. Appl Phys Lett 2002;81(358):358–60.
[7] Taniyasu Yoshitaka, Kasu Makoto, Makimoto Toshiki. Field emission properties of heavily Si-doped AlN in triode-type display structure. Appl Phys Lett 2004;84(2115):2115–7.
[8] Choi YS, Cho YS, Kang JH, Kim YJ, Kim IH. A field-emission display with a self-focus cathode electrode. Appl Phys Lett 2003;82(20):3565–7.

[9] Choi Young Chul, Jeong Kwang Seok. Double-gated field emitter array with carbon nanotubes grown by chemical vapor deposition. Appl Phys Lett 2006;88(263504):1–3.
[10] Dvorson Leonard, Akinwande Akintunde I. Double-gated Spindt emitters with stacked focusing electrode. J Vac Sci Technol B 2002;20(1):53–9.
[11] Wang XQ, Wang M, Ge HL, Chen Q, Xu YB. Modeling and simulation for the field emission of carbon nanotubes array. Physica E 2005;30:101–6.
[12] Li Y, Cheng H-W. Numerical simulation of field emission efficiency of anodic aluminum oxide carbon nanotube field emitter in the triode structure. Comput Phys Commun; 2008:107–11.
[13] Deng Min, Ding Guifu, Wang Yan, Wang Yuchao, Wang Hong, Fu Shi. MEMS-based carbon nanotube and carbon nanofiber Cu micro special electric contact. J Micromech Microeng 2009;19(065001):1–8.